Chapter 1

Thermodynamics of the Atomic and Molecular Gas

Inga Kamp[1], *Daniele Galli*[4], *Christian Rab*[2,3]

[1]*Kapteyn Astronomical Institute, University of Groningen, PO Box 800, 9700 AV Groningen, The Netherlands,*
[2]*Universitäts-Sternwarte, Fakultät für Physik, Ludwig-Maximilians-Universität München, Scheinerstr. 1, 81679 München, Germany,*
[3]*Center for Astrochemical Studies, Max-Planck-Institut für Extraterrestrische Physik, Giessenbachstrasse 1, D-85748, Garching, Germany,*
[4]*INAF Osservatorio Astrofisico di Arcetri, Largo E. Fermi 5, 50125 Firenze, Italy*

ABSTRACT

Each phase of the ISM has a temperature that results from a balance of heating and cooling. These processes differ from place to place in the Galaxy and vary with time. Under particular conditions, the resulting thermal equilibrium can be unstable and promote the separation of coexisting thermodynamic phases in pressure equilibrium with each other. Determining the temperature is a big challenge for numerical modeling as many different microphysical processes have to be considered, and usually, simplifying assumptions have to be made. This chapter discusses the most important known heating and cooling processes for various physical conditions (i.e., from the diffuse ISM to planet-forming disks). We provide the necessary equations and references to the required data but also discuss simplified methods and their assumptions for each process. We conclude with a brief description of how to solve the heating/cooling balance considering different levels of complexity.

KEYWORDS

heating:photons, heating:cosmic rays, cooling:radiative

Each phase of the ISM has a temperature that results from a balance of heating and cooling. These processes differ from place to place in the Galaxy, and vary with time. Under particular conditions, the resulting thermal equilibrium can be unstable, and promote the separation of coexisting thermodynamic phases in pressure equilibrium with each other. Most heating process involve the production of electrons with suprathermal energies, which are quickly thermalized by collisions with the ambient medium. These electrons may have been ejected from atoms, molecules or dust grains by photons (Sect. 1.1.1 and 1.1.2), cosmic rays (Sect. 1.1.3), or X rays (Sect. 1.1.4). Alternatively, a fraction of the kinetic energy of orderly bulk flows like stellar winds and shocks, or disturbances like

MHD waves, or turbulent cascades can be converted into thermal energy of ambient particles (Sect. 1.1.5). Heating in the ISM can also result from exothermic chemical reactions, like, e.g., the formation of H_2 on the surface of dust grains (Sect. 1.1.6).
The ISM presents also a wide variety of cooling processes. Past supernova shocks, rapid adiabatic cooling works by changing gas pressure via volume expansion (Sect. 1.2.1), while in hot, highly ionized gas, energy is mostly radiated away by free-free emission (Sect. 1.2.2) and radiative recombination (Sect. 1.2.3). The dominant cooling process at lower temperatures is radiative line cooling, whereby collisional excitation of energy levels of atoms or molecules is followed by the spontaneous emission of a photon that can escape the medium, rather than be reabsorbed (Sect. 1.2.4).
In this chapter we will consistently use the standard notation, whereby the *volumetric heating and cooling rates* (energy gained/lost per unit volume and unit volume, in erg cm^{-3} s^{-1}) are denoted by Γ and Λ, respectively, while the frequently used and tabulated *heating/cooling functions* (in erg cm^3 s^{-1}) are denoted by $\mathcal{G}$ and $\mathcal{L}$, respectively. Below is a list of heating and cooling processes in various astrophysical media.

Medium	Heating	Cooling
MC	photoelectric eff.; cosmic rays	radiative (CO, H_2, OI, H_2O), dust
CNM	photoionization of C; photoelectric eff.	radiative (CII, OI)
WNM	photoionization of C; photoelectric eff.	radiative(CII, OI, Ly-α)
HIM	shocks	adiabatic expansion, X-ray emission
H II region	photoionization of H, He	recombination of H and He, free-free
PFD	see Chap. **??**	see Chap. **??**

TABLE 1.1 Relevance of heating/cooling processes for various media: Molecular Cloud (MC), Photon-dominated Region (PDR), Cold Neutral Medium (CNM), Warm Neutral Medium (WNM), Hot Ionised Medium (HIM), HII region, Planet-Forming Disk (PFD).

1.1 HEATING PROCESSES

1.1.1 Photoionization heating

Photoionization is an important, often dominant, heating process in the gas surrounding radiation sources emitting photons of energy sufficient to ionize atoms and ions, as in HII regions and photodissociation regions. As a reference, the ionization potentials of the most abundant atoms are $I_H = 13.60$ eV, $I_{He} = 24.59$ eV, $I_C = 11.26$ eV, $I_N = 14.53$ eV, $I_O = 13.62$ eV. Molecular hydrogen has a ionization potential $I_{H_2} = 15.43$ eV. The electrons ejected in the ionization events ("photoelectrons") have sufficient energy to collisionally excite (or even ionize) other species, and to transfer momentum to the ambient medium, raising its temperature (for more details see also Chap. **??**. The net result is the conversion of radiative energy of stars into thermal energy of gas.

The rate of photoionization (in s^{-1}) of an atom, ion, or molecule X^r with threshold energy $h\nu_0$ is

$$\zeta_{\rm ph}(X^r) = \int_{\nu_0}^{\infty} \frac{4\pi J_\nu}{h\nu} \sigma_\nu(\mathrm{X}^r)\, \mathrm{d}\nu, \tag{1.1}$$

where $h\nu$ is the photon energy, $\sigma_\nu(X^r)$ is the photoionization cross section of species X^r, and J_ν is the mean specific intensity of the radiation field[1] (erg cm^{-2} s^{-1} Hz^{-1}) (see, e.g. Osterbrock & Ferland 2006). The radiation field should of course include the modifications induced by absorption and scattering of the ambient medium on the emission of the sources, and the emission of the ionized gas itself. Photoionization cross sections of hydrogenic atoms with atomic number Z are well approximated by a power-law behavior in the photon energy,

$$\sigma_\nu \approx \sigma_1 x^{-3} \ \text{ for } 1 \lesssim x \lesssim 10^2, \qquad \sigma_\nu \approx \sigma_2 x^{-3.5} \ \text{ for } x \gg 10^2, \tag{1.2}$$

where $x = h\nu/(Z^2 I_{\rm H})$, $\sigma_1 = 6.304 \times 10^{-18} Z^{-2}$ cm^2 and $\sigma_2 = 5.478 \times 10^{-17} Z^{-2}$ cm^2 (see, e.g., Draine 2011). Convenient analytic fits of photoionization cross sections are given by Verner & Yakovlev (1995) and Verner et al. (1996) for atoms and by Yan et al. (2001) and Liu & Shemansky (2012) for H_2. Photoionization cross sections of several molecules of astrophysical interest can be found in Heays et al. (2017) and are also available from the Leiden database (see Chap. **??** and **??** for more details).

Because of the very large electron-electron cross sections, photoelectrons thermalize very quickly, converting their initial kinetic energy $h(\nu - \nu_0)$ into thermal energy of the gas. The volumetric heating rate from photoionization (in erg cm^{-3} s^{-1}) is then

$$\Gamma_{\rm ph}(X^r) = n(X^r) \int_{\nu_0}^{\infty} \frac{4\pi J_\nu}{h\nu} h(\nu - \nu_0) \sigma_\nu(\mathrm{X}^r)\, \mathrm{d}\nu, \tag{1.3}$$

where $n(\mathrm{X}^r)$ is the number density of species X^r. The species contributing to ionization heating depend on the spectral energy distribution of the source and the composition of the medium: photons with energy $I_{\rm H} < h\nu < I_{\rm He}$ can ionize H only, photons with energy $h\nu > I_{\rm He}$ can ionize H and He, and photons with energy $h\nu < I_{\rm He^+} = 54.42$ eV can also ionize He^+. However, photons with energy $h\nu > I_{\rm H}$ are only found in HII regions, planetary nebulae, and in general in the WIM. Outside of these environments, in practice, only C can be ionized. Thus, in neutral regions photoionization of the gas becomes rather inefficient, and dust grains become the main source of photoelectrons (see Sect. 1.1.2).

1. The mean specific intensity can be expressed in terms of the energy density per frequency interval u_ν of the radiation field, $4\pi J_\nu = u_\nu c$, where c is the speed of light.

1.1.2 Photoelectric heating

1.1.2.1 General concepts

Photoelectric emission from dust grains and PAHs is the dominant heating process in the cold neutral medium (Watson 1972; Glassgold & Langer 1974; Draine 1978; Bakes & Tielens 1994) and plays also a role in the surfaces of planet-forming disks (Kamp & Dullemond 2004; Jonkheid et al. 2004; Woitke et al. 2009). In the following, we distinguish between larger dust grains (silicate and carbonaceous bulk solids) and small PAHs.

Ultraviolet photons from the interstellar radiation field absorbed by dust grains can create energetic electrons that diffuse and escape from the grain's surface if they have sufficient energy to overcome the potential energy barrier. The energy needed to remove an electron from the surface of a solid is called the *work function* W (e.g., for graphite, $W = 4.50$ eV and for silicates, $W = 8.0$ eV, Weingartner & Draine 2001b). The process is therefore similar to photoionization heating, with the work function playing the role of the ionization energy of an atom. However, the efficiency of electron removal from a dust grain also depends on the charge state of the grain. For a grain of radius a, and charge Z_g is convenient to define an ionization potential

$$I_g = W + \left(Z + \frac{1}{2}\right)\frac{e^2}{a} + (Z+2)\frac{e^2}{a}\left(\frac{0.3\ \text{Å}}{a}\right), \tag{1.4}$$

where the second and third terms are due to the electron having to overcome the Coulomb potential ($Z \geq 0$) and the effect of extra electrons in the lowest unoccupied molecular orbital ($Z < 0$) (Weingartner & Draine 2001b). Calculating the photoelectric heating involves then evaluating the ionization and recombination rates for a grain self consistently to find the equilibrium charge state of the grain Z_g (see Ch. 9). Once ejected into the ambient medium, photoelectrons thermalize with free electrons, releasing their kinetic energy in the form of heat. The rate of emission of photoelectrons (in s^{-1}) by this process is

$$\zeta_{\text{pe}} = \int_0^\infty \frac{4\pi J_\nu}{h\nu}\sigma_{\text{abs}} Y_{\text{pe}}\, \text{d}\nu, \tag{1.5}$$

where J_ν is the mean specific intensity of the radiation field (in $\text{erg cm}^{-2}\,\text{s}^{-1}\,\text{Hz}^{-1}$), $\sigma_{\text{abs}} = q_{\text{abs}}\pi a^2$ is the grain absorption cross section (see Chap. **??** for additional details), and Y_{pe} is the *photoelectric yield*, the probability that the absorption of a photon results in the emission of a photoelectron. The *absorption coefficient* q_{abs} and the photoelectric yield Y_{pe} depend on the energy of the photon and the size and composition of the grain; in addition, Y_{pe} also depends on the charge state of the dust grain (Weingartner & Draine 2001b; Weingartner et al. 2006). Figures showing how q_{abs} and Y_{pe} change with grain size and material are given by Draine (2011). Weingartner & Draine (2001b) note however that the yields for silicate and carbonaceous grains (and PAHs) are highly uncertain. Appro-

priate laboratory measurements are lacking and often a simple semi-empirical formalism is used.

PAHs can be either considered as very small grains with bulk properties or very large molecules depending on the physical/chemical process under consideration. For the ionization, detailed PAH absorption cross sections σ have been provided by Draine & Li (2001) and Draine & Li (2007) for neutral and ionized PAHs. For deriving the charge balance of PAHs, we again refer to Chap. **??**. Once the charge of the PAHs is known, the rate of emission of photoelectrons is calculated in the same way as for dust grains, but adopting the appropriate values for the ionization potential and yield, both of which depend on the number of C-atoms within the PAH (Bakes & Tielens 1994).

Both for grains and PAHs an extra complication arises from the fact that the charge balance can be affected by charge exchange reactions within the chemistry. This means that not only electron and proton collisions affect the charge balance of grains and PAHs, but also reactions with metal ions such as C^+, Si^+, Fe^+, and molecular ions such as H_3O^+, NH_4^+, and HCO^+ (e.g., Flower & Pineau des Forêts 2003; Wolfire et al. 2008).

Assuming that half of the excess energy of the incident photon is carried by the ejected photoelectron (the other half being dissipated in the internal excitation of the grain), the volumetric heating rate from photoelectric emission (in erg cm^{-3} s^{-1}) is

$$\Gamma_{\rm pe} = \frac{1}{2} n_{\rm d} \int_0^\infty \frac{4\pi J_\nu}{h\nu} \sigma_{\rm abs} Y_{\rm pe}(h\nu - I_{\rm g})\, {\rm d}\nu. \tag{1.6}$$

where $n_{\rm d}$ is the volume density of dust grains. However, the reverse process must be taken into account: the recombination of ambient electrons onto dust grains represents an energy loss for the gas of $(3/2)k_{\rm B}T$ per recombination (*recombination cooling*, $\Lambda_{\rm rec}$).

The detailed evaluation of the net heating rate $\Gamma_{\rm pe} - \Lambda_{\rm rec}$ is clearly dependent on the knowledge of several quantities, like the grain composition, size distribution, and charge state. The problems of determining grain charges and the net photoelectric heating rate become thus a coupled problem.

1.1.2.2 Numerical implementation

For several types of astrophysical environments and grain properties, this problem has been solved and much simpler analytical rates can be found in the literature. An example is the approximated analytical expression for the photoelectric heating rate (in erg cm^{-3} s^{-1}) derived by Bakes & Tielens (1994) for small carbonaceous grains (3.1×10^{-4} μm $< a < 10^{-2}$ μm) and PAHs in the warm and cold neutral medium and in strongly irradiated PDRs,

$$\Gamma_{\rm pe} \approx 10^{-24} G_0 \epsilon n_{\rm H}, \tag{1.7}$$

where G_0 represents the enhancement of the radiation field with respect to the Habing field, and

$$\epsilon = \frac{4.87 \times 10^{-2}}{1 + 4 \times 10^{-3} (G_0 T^{1/2}/n_e)^{0.73}} + \frac{3.65 \times 10^{-2} (T/10^4\ \mathrm{K})^{0.7}}{1 + 2 \times 10^{-4} (G_0 T^{1/2}/n_e)}; \tag{1.8}$$

Similarly, the recombination cooling rate is approximated as

$$\Lambda_{\mathrm{rec}} \approx 3.49 \times 10^{-30} T^{\alpha} (G_0 T^{1/2}/n_e)^{\beta} n_e n_{\mathrm{H}}, \tag{1.9}$$

where $\alpha = 0.944$ and $\beta = 0.735 (T/\mathrm{K})^{-0.068}$. Bakes & Tielens (1994) show that for low density ($n_{\mathrm{H}} < 1\ \mathrm{cm}^{-3}$) ISM conditions, the recombination cooling rate becomes important only for high temperatures ($T > 5000$ K).
Weingartner & Draine (2001b) use ISM size distributions for both carbonaceous and silicate grains (taken from Weingartner & Draine 2001a) to estimate the total net photoelectric heating rate for a blackbody spectrum ($T_{\mathrm{c}} = 3 \times 10^4$ K) and the typical ISRF. They derive an analytical approximation for the net volumetric heating rate (erg $\mathrm{cm}^{-3}\ \mathrm{s}^{-1}$):

$$\Gamma_{\mathrm{pe}}^{\mathrm{net}} \approx 10^{-26} G_0 \epsilon n_{\mathrm{H}}, \tag{1.10}$$

with an efficiency of

$$\epsilon = \frac{C_0 + C_1 T^{C_4}}{1 + C_2 (G_0 \sqrt{T}/n_e)^{C_5} [1 + C_3 (G_0 \sqrt{T}/n_e)^{C_6}]}. \tag{1.11}$$

Here, the coefficients C_0 to C_6 are provided in tabular form for a range of radiation fields, grain size distributions parametrized in terms of the total-to-selective extinction R_V and carbon abundance in grains b_{C}. Similarly to Bakes & Tielens (1994), they also conclude that the recombination cooling (erg $\mathrm{cm}^{-3}\ \mathrm{s}^{-1}$) is mostly important at high temperatures ($T \gtrsim 10^3$ K),

$$\Lambda_{\mathrm{rec}} \approx 10^{-28} n_e n_{\mathrm{H}} T^{D_0 + D_1/x} \exp(D_2 + D_3 x - D_4 x^2), \tag{1.12}$$

with $x = \ln(G_0 \sqrt{T}/n_e)$. Again, the coefficients D_0 to D_4 are tabulated for various radiation fields, grain size distributions and carbon abundances.

1.1.2.3 Application to planet-forming disks

Under certain conditions, the contribution of the small grains dominates photoelectric heating. It is important to note that the grain size distributions in planet-forming disks deviate notably from that of Weingartner & Draine (2001a) and also Bakes & Tielens (1994). Dust grain growth and settling processes will lead to a vertical size sorting in disks, leaving the surface mostly populated by small dust grains. However, in that case, the abundance of those small grains per H-atom has to be taken into account properly to be able to use the above formulas. An additional complication is that the above approximations have the

shape of the radiation field built in. While the G_0 parameter allows to some extent the scaling of such radiation fields, one has to be careful to (*i*) not use the formulas outside the range of validity (temperature and charging parameter) and (*ii*) not use them for radiation fields with very different spectral shape, e.g. in planet-forming disks around cool stars.

Various approaches have been used in the disk literature to include the above effects. For example, Du & Bergin (2014) scale the rate by the dust-to-gas mass ratio relative to that of the ISM, a factor 0.01; Aikawa & Nomura (2006) use a similar approach of scaling. On the other hand, Gorti & Hollenbach (2004) noted this problem and obtained from Weingartner (private communication) size-dependent efficiencies for various black body temperatures to calculate the grain photoelectric heating. Jonkheid et al. (2004) use full 2D radiative transfer to derive the charge state of grains and PAHs and deduce the corresponding heating rates using a simple analytical formula from Tielens & Hollenbach (1985) for small grains and scaling it for a varying dust-to-gas ratio. Kamp & van Zadelhoff (2001) generalized the formalism of Draine (1978) to large micron-sized dust grains and provided an approximation for the photoelectric heating of carbonaceous and silicate grains.

1.1.3 Cosmic-ray heating

Cosmic rays are an important source of heating in various environments, from diffuse atomic regions to the dense gas in molecular clouds. The volumetric CR heating rate (in erg cm^{-3} s^{-1}) is usually parametrized as

$$\Gamma_{\rm CR} = \zeta_{\rm H} Q n_{\rm H}, \tag{1.13}$$

where $n_{\rm H} = n({\rm H}) + 2n({\rm H_2})$ is the total H density, $\zeta_{\rm H}$ is the CR ionization rate (in s^{-1}) per H atom, including secondary ionizations (see Chap. **??**), and Q is the average heat deposited in the gas per ionization (Spitzer & Tomasko 1968; Glassgold & Langer 1973). Since each CR ionization produces an ion and a distribution of relatively slow electrons, the calculation of Q must take into account all energy loss channels for the secondary electrons as well as the chemical heating released by chemical reactions of the generated ions with the ambient atomic and molecular species.

In the neutral atomic regions of the CNM, the secondary electron loses energy in ionizations and excitations of H and He until its energy falls below the hydrogen Ly-α energy of 10.20 eV. The remaining energy is then lost in elastic collisions. These conclusions are not significantly dependent on the composition of the medium. The addition of a 10% He fraction to a pure H gas increases the amount of heat deposited by secondary electrons by less than 2% (Dalgarno et al. 1999). The fraction of metals in the gas contributes much less. The amount of heat released in the atomic gas, $Q_{\rm at}$, depends however crucially on the ionization fraction of the medium, as shown at the end of this subsection.

Detailed calculations give values of $Q_{\rm at}$ ranging from $Q_{\rm at} = 5.7$ eV (Spitzer

& Tomasko 1968) to 8.5 eV (Field et al. 1969), but we recommend the value $Q_{\rm at} = 4.3$ eV computed by Glassgold et al. (2012). Chemical heating resulting from reactions of H^+ and He^+ with ambient species is negligible (Glassgold et al. 2012).

In molecular regions, the diversity of the energy levels of H_2 offers many more channels for energy loss than atomic H. Secondary electrons lose energy mainly in ionization of H_2 and He, and excitation of bound states of H_2 and He that can be collisionally deexcited at high densities, heating the gas. As a consequence, the amount of heat deposited in molecular gas, $Q_{\rm mol}$, is an increasing function of the ambient density. Chemical heating, mostly from reactions of H_2^+ with other molecules, contributes significantly to $Q_{\rm mol}$, especially at high densities. Fig. 1.1 shows the value of $Q_{\rm at}$ e $Q_{\rm mol}$ (in eV) computed by Glassgold et al. (2012) for a neutral mixture of H or H_2 and He.

In a partially ionized medium, the CR heating increases significantly above the values shown in Fig. 1.1 due to Coulomb collisions of secondary electrons with ambient electrons. The fraction of electron kinetic energy converted into thermal energy is about 10% for a fractional ionization $x_e \approx 10^{-4}$, and above 70% for $x_e \approx 0.1$. Numerical values and analytic fits of the fraction of electron kinetic energy converted into heating as a function of the ionization fraction x_e are given by Shull & van Steenberg (1985), Xu & McCray (1991), Furlanetto & Stoever (2010). Draine (2011) gives a simple approximate expression to estimate the contribution to the energy deposited in the gas by electron-electron collisions Q_{ee}, to be added to the value of $Q_{\rm at}$ shown in Fig. 1.1,

$$Q_{ee} \approx 24.6 \left(\frac{x_e}{x_e + 0.07} \right)^{1/2} \text{ eV}. \tag{1.14}$$

For example, $Q_{ee} \approx 0.9$ eV in a PDR with $x_e \approx 10^{-4}$, and the total heat deposited in the gas per ionization is $Q = Q_{\rm at} + Q_{ee} \approx 5.2$ eV.

1.1.4 X-ray heating

T Tauri stars show high X-ray luminosities of typically $L_{\rm X} \approx 2 \times 10^{30}\,{\rm erg\,s^{-1}}$ and X-rays can therefore be an important heating agent for protoplanetary disks and in studies of galaxies and galaxy clusters. X-ray ionization of atoms and molecules produces secondary electrons that partly further ionize the medium but also transfer their energy into heat. This process is often called X-ray Coulomb heating. This is a similar process as for cosmic rays, and therefore similar concepts can be applied to calculate the X-ray heating rate (see 1.1.3). Following Dalgarno et al. (1999) the X-ray Coulomb heating rate in units ${\rm erg\,cm^{-3}\,s^{-1}}$ can be expressed as

$$\Gamma_{\rm X} = n_{\rm H} \eta H_{\rm X}\,, \tag{1.15}$$

where η is the heating efficiency and $H_{\rm X}$ is the X-ray energy deposition per hydrogen nuclei. The parameter η depends on the composition of the gas;

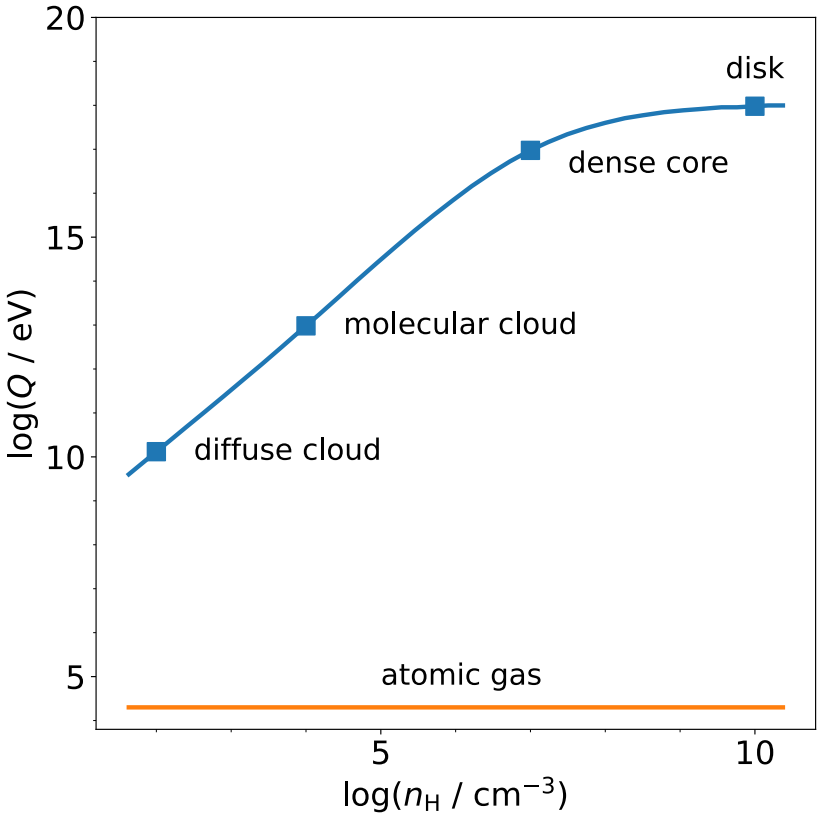

FIGURE 1.1 Average heat input Q per CR ionization as a function of the total H density $n_{\rm H}$ (adapted from Glassgold et al. 2012). Bottom curve, $Q_{\rm at}$; top curve, $Q_{\rm mol}$.

for a mixture of atomic/molecular hydrogen and He it can be approximated by (Dalgarno et al. 1999, Eq. 12)

$$\eta = \frac{10r\eta_{\rm H_2\,He} + \eta_{\rm H\,He}}{10r + 1}\,. \tag{1.16}$$

Here, $r = n({\rm H_2})/n({\rm H})$ is the H_2 and H number density ratio, and $\eta_{\rm H_2\,He}$, $\eta_{\rm H\,He}$ are efficiencies for pure H_2 and He and H and He mixtures, respectively. For those quantities fitting formulas as a function of energy derived from theoretical calculations are used (see e.g., Dalgarno et al. 1999; Glassgold et al. 2012). A typical number for an H_2 dominated gas mixture assuming a typical X-ray energy of $E = 1$ keV is $\eta = 0.055$ (Glassgold et al. 2012).
The X-ray energy deposition $H_{\rm X}$, in erg $\langle {\rm H}\rangle^{-1}$, is

$$H_{\rm X}(E) = \int \sigma_{\rm tot}(E) F_{\rm X}(E) {\rm d}E\,, \tag{1.17}$$

where $\sigma_{\rm tot}$ is the total absorption (i.e. all considered chemical species)[2] cross section and $F_{\rm X}(E)$ is the local X-ray radiation flux in units of erg cm^{-2} s^{-1} eV^{-1}. To evaluate $H_{\rm X}$ the X-ray cross sections of the atoms and molecules and the local X-ray radiation need to be known. For the X-ray gas absorption cross sections, the analytic fits of Verner et al. (1996) are often adopted, however they do not include scattering cross sections nor X-ray dust opacities. Depending on the application the latter processes might be quite relevant. For example, X-ray scattering can be quite an important process for ionization in the midplane of protoplanetary disks, depending on the actual cosmic ray ionization rates (e.g., Cleeves et al. 2015). A more complete tool to calculate X-ray cross sections is the freely available library XRAYLIB[3] (Schoonjans et al. 2011), which provides easy-to-use routines to evaluate both the absorption and scattering cross sections of many atomic and molecular species.
For the dust usually also the gas absorption cross sections are used and it is simply assumed that the considered species are in the solid form (e.g., Bethell & Bergin 2011). However, to also evaluate dust scattering opacities proper optical constants need to be calculated. A numerical method to do that is presented in Draine (2003). On top of that, e.g., the Mie theory can be used to calculate the actual dust opacities as extensively discussed in Chap. **??**. Generally speaking, calculating X-ray dust opacities is a complex and expensive task, but often not necessary especially if the environment is gas dominated (for more details see Rab et al. 2018). To calculate the local X-ray radiation field including scattering proper radiative transfer methods are required (e.g., Igea & Glassgold 1999; Rab et al. 2018). In case scattering can be neglected it is only required to calculate the X-ray absorption along rays towards the light source (e.g., a T Tauri star), like in Aresu et al. (2011). One challenge in this process is to calculate the radiation field consistently with the chemistry as for example atomic, molecular hydrogen, or metals can be efficiently ionized by X-rays (e.g., Ercolano et al. 2008; Rab et al. 2018). However, a simpler treatment considering only a neutral medium is often a reasonable approximation for calculating the X-ray ionization rate, if the medium is only weakly ionized.

1.1.5 Mechanical heating

Mechanical heating arises from the conversion of a fraction of the kinetic energy of orderly bulk flows, turbulent cascades, wavelike disturbances, into thermal energy associated with random particle motion. This conversion may occur in the form of continuous energy dissipation (viscous heating and ambipolar diffusion heating) or mediated by discontinuities in the flow called shock waves (shock heating).

2. Here $\sigma_{\rm tot} = \sum_i \sigma^i_{\rm pe}$, see Chap. **??**.
3. https://github.com/tschoonj/xraylib

1.1.5.1 Viscous heating

The energy release associated with ordinary microscopic fluid viscosity is generally negligible in the ISM. In classical accretion disk theory (Pringle 1981), the outward transfer of angular momentum and the inward flow of mass is attributed to the presence of an anomalous (turbulent) viscosity, usually parametrized by the so-called α prescription (Shakura & Sunyaev 1973),

$$\nu = \alpha c_{\rm s} H, \tag{1.18}$$

where ν is the viscosity coefficient (units of cm^2 s^{-1}), $c_{\rm s}$ is the sound speed in the gas, and H is the vertical disk scale height. However, the origin of turbulence in disks around protostars and compact objects (if present at all) is still debated. In a viscous disk, the energy dissipated per unit of time and unit volume is

$$\Gamma_{\rm vis} = \nu\rho \left(R \frac{{\rm d}\Omega}{{\rm d}R} \right)^2, \tag{1.19}$$

where ρ is the gas density and Ω is the angular rotation speed. Eliminating the disk scale height $H = c_{\rm s}/\Omega$ from Eq. (1.18) and assuming Keplerian rotation ($\Omega \propto R^{-3/2}$), Eq. (1.19) can be written as

$$\Gamma_{\rm vis} = \frac{9}{4} \nu\rho\Omega^2. \tag{1.20}$$

It is important to note that implementing Eq. (1.20) in 2D disk models can lead to a "heating catastrophe" in the case of a gas density approaching low values in the surface or outer disk. For this reason is convenient to integrate Eq. (1.20) over the vertical thickness of the disk to obtain the heating rate per unit surface area,

$$\int \Gamma_{\rm vis}\, {\rm d}z = \frac{3}{4\pi} \dot{M}\Omega^2, \tag{1.21}$$

where $\dot{M} = 3\pi\nu\Sigma$ is the (constant) mass accretion rate through the disk (Pringle 1981), with Σ being the gas surface density. Viscous heating, also called accretion heating, represents an important source of energy in the inner regions ($R \lesssim 2$ au) of protostellar disks (D'Alessio et al. 1998).

1.1.5.2 Ambipolar diffusion and Ohmic heating

In a partially ionized medium like a molecular cloud or a protostellar wind/jet, a source of heating for the gas is represented by the friction between neutral and charged particles due to velocity drifts induced by the slippage of the magnetic field, a process called in astrophysics *ambipolar diffusion heating* (Scalo 1977). At higher densities, *Ohmic heating* due to the dissipation of electric currents by collisions must also be taken into account. Expression for the heating rate per unit volume $\Gamma_{\rm ad}$ and $\Gamma_{\rm O}$, corresponding to the two processes, can be found in Chap. 2.

1.1.5.3 Shock heating

Shock waves play an important role in the dynamics of the present-day ISM, and in the formation of large-scale structures in the early Universe. The hot and warm ionized medium are heated by shocks generated by phenomena like supernova explosions, stellar winds, expansion of HII regions, but shocks are also expected to arise in the process of gravitational collapse (accretion shocks), in the interaction of protostellar jets with the ambient medium (bow shocks) and inside the jets themselves, when fast fluid elements catch up with slower ones (internal shocks).

The energy dissipated by a shock depends on the properties of the ambient medium and on the properties of the shock, most notably the *shock strength* $\xi = \Delta p/p_0$, the ratio of excess pressure just behind the shock front to the unperturbed pressure p_0. The shock strength can be expressed in terms of the Mach number $\mathcal{M}$ of the shock as $\xi = 2\gamma(\mathcal{M}^2 - 1)/(\gamma + 1)$, where γ is the adiabatic index. The volumetric heating rate (in erg cm^{-3} s^{-1}) produced by the complete dissipation of a stream of weak ($\mathcal{M} \gtrsim 1$) plane shock waves injected at a rate ν_s into a region of the ISM is proportional to the third power of the shock strength,

$$\Gamma_s = \nu_s \frac{1+\gamma}{12\gamma^2} p_0 \xi^3, \tag{1.22}$$

(Schatzman 1949; Weymann 1960).

Strong shocks produced by SNe (and expanding ionized envelopes of massive stars) are very efficient in heating to high temperatures the low-density gas filling about half of the volume of the galactic disk and much of the volume above and below the disk. The temperature behind a strong adiabatic shock propagating with speed v_s is

$$T \approx \frac{2(\gamma-1)}{(\gamma+1)^2} \frac{\mu m_H}{k_B} v_s^2, \tag{1.23}$$

or $T \approx 10^7$ K for $\gamma = 5/3$ and $u_s \approx 10^3$ km s^{-1}. The energy input by SNe occurring at a rate ν_{SN} in a volume V provides a volumetric heating rate (in erg cm^{-3} s^{-1})

$$\Gamma_{SN} = \nu_{SN} \frac{\epsilon E_{SN}}{V}, \tag{1.24}$$

where E_{SN} is the energy released by a SN and ϵ is the fraction of this energy released in the form of thermal energy to the ambient medium. There is a varying degree of uncertainty in our knowledge of the above parameters: $E_{SN} \approx 10^{51}$ erg within a factor of ~ 2 depending on the mass of the supernova; $\epsilon \approx 0.1$, the rest of the SN energy being lost to radiation (Thornton et al. 1998); the SN rate is a function of time, with a current value $\nu_{SN} \approx 0.02$ yr^{-1} over the full volume of the Galaxy (see, e.g., Rozwadowska et al. 2021).

The modelization of shocks in numerical simulation is not straightforward, since their characteristics (or even occurrence at all) depend on the code's resolution, viscosity, numerical scheme adopted, etc. (for a review, see, e.g., Dolag

et al. 2008). For example, in Smoothed Particle Hydrodynamics (SPH) codes, shock heating is realized by introducing an artificial viscosity active only when fluid elements approach one another in space, preventing particle interpenetration and transforming kinetic energy irreversibly into heat (Monaghan & Gingold 1983). Conversely, Eulerian numerical schemes adopting the Piecewise Parabolic Method (PPM, Woodward & Colella 1984), or the Total Variation Diminishing scheme (TVD, Harten & Hyman 1983), shocks are treated accurately by solving the Riemann problem through explicit methods. The Rankine-Hugoniot shock conditions allow to evaluate the effective shock Mach number M in numerical simulations via either *velocity-based* methods or *temperature-based* methods by measuring the jump in the fluid velocity v

$$\frac{v_2}{v_1} = \frac{M^2+3}{4M^2}, \tag{1.25}$$

or in the temperature T

$$\frac{T_2}{T_1} = \frac{(5M^2-1)(M^2+3)}{16M^2}, \tag{1.26}$$

respectively (here an adiabatic index $\gamma = 5/3$ has been assumed).

1.1.6 Chemical heating

Exothermic chemical reactions release energy that can be converted into heat. Here we describe an approximate method for including this chemical heating processes in the heating and cooling balance. Following Woitke et al. (2011) the chemical heating rate is

$$\Gamma_{\rm chem} = \sum_r R(r)\gamma_r^{\rm chem}\Delta H_r\,, \tag{1.27}$$

where $\Gamma_{\rm chem}$ is in $\mathrm{erg\,cm^{-3}\,s^{-1}}$, $R(r)$ is the reaction rate in $\mathrm{cm^{-3}\,s^{-1}}$ of a chemical reaction with index r (see also Sect. **??**), and $\gamma_r^{\rm chem}$ is an efficiency parameter (will be described later on). The reaction enthalpy ΔH_r (in erg) is given by

$$\Delta H_r = \sum_{\rm pr}\Delta H_f^0(pr) - \sum_{\rm re}\Delta H_f^0(re)\,, \tag{1.28}$$

where H_f^0 is the heat of formation (or enthalpy of formation) of a particular chemical species at $T = 0\,\mathrm{K}$. Here H_f^0 needs to be know for each product pr and reactant re of the chemical reaction r. Some data for the heat of formation can be found in the KIDA or UMIST chemical databases for particular temperatures. A more comprehensive list for $T = 0\,\mathrm{K}$ is provided by the NIST Computational Chemistry Comparison and Benchmark DataBase[4] and also by ATcT (Active Thermochemical Tables)[5]. There is also data available for temperature-

4. https://cccbdb.nist.gov/hf0k.asp
5. https://atct.anl.gov/

dependent H_f, which are usually expressed in polynomials. A comprehensive explanation is for example provided by Alexander Burcat[6]. There also exist some easier-to-use and free python tools that combine temperature-dependent data from Burcat and others such as thermochem[7].

1.1.6.1 Photochemical Heating

Besides the radiation-driven photoionization heating (Sect. 1.1.1) also heating by photodissociation can play a relevant role in dense molecular regions such as molecular clouds and protoplanetary disks. However, this process is often not considered and not fully explored.

According to Glassgold & Najita (2015) the actual heating yield driven by photoionizatoin or photodissociation can be dominated by chemical heating. Meaning the resulting chemical reactions induced by these processes yield more heating energy than the energy released due to the direct interaction of the photons with molecules. The resulting chemical products of photoionizatoin/dissociation are often excited and this excitation energy can be converted to heating. However, the actual amount of released energy is uncertain and depends on the molecule, but can be in the range of 1 to 10 eV per interaction, for molecules such as H_2, CO, and H_2O (see Table 7 in Glassgold & Najita 2015 for more detailed numbers).

1.1.6.2 H_2 formation heating

A special case of chemical heating is the formation of H_2. It can occur in the gas phase by associative detachment, $H + H^- \rightarrow H_2 + e^-$, with $\Delta H_r = 3.75$ eV (Le Teuff et al. 2000). If H_2 is formed in the ground state, this formation energy is carried by the ejected electron, and the heating rate is given by Eq. (1.27) above. This is mostly relevant in environments with low dust content, e.g. the early universe.

If the formation of H_2 occurs on the surface of dust grains, an amount of energy equal to the binding energy of H_2, $E_{HH} = 4.50$ eV, is released. Writing the rate of H_2 formation by grain catalysis as (Draine 2011)

$$\left[\frac{\mathrm{d}n(\mathrm{H_2})}{\mathrm{d}t}\right]_{\mathrm{gr}} = R_{\mathrm{gr}} n_{\mathrm{H}} n(\mathrm{H}), \tag{1.29}$$

where R_{gr} is an effective rate coefficient, the H_2 formation heating (in erg cm^{-3} s^{-1}) in this case is

$$\Gamma_{\mathrm{form}} = R_{\mathrm{gr}} n_{\mathrm{H}} n(\mathrm{H}) \langle E_{\mathrm{form}} \rangle, \tag{1.30}$$

where $\langle E_{\mathrm{form}} \rangle$ is the energy released in the formation process that goes into gas heating. The partitioning of the released energy is not well known: a fraction f_{gr} goes into heating of the grain, a fraction f_{int} into internal energy

6. https://burcat.technion.ac.il/dir/
7. https://github.com/adelq/thermochem

(rotational and vibrational excitation), and a fraction $f_{\rm kin}$ into kinetic energy of H_2. A common assumption based on equipartition is that $f_{\rm gr} \approx f_{\rm int} \approx f_{\rm kin} \approx 1/3$ and that the kinetic energy of the newly formed H_2 is converted into heating, $\langle E_{\rm form}\rangle \approx f_{\rm kin} E_{\rm HH} = 1.50$ eV (see, e.g. Liszt 2007). Classical molecular dynamics calculations of the Eley–Rideal recombination of H atoms on graphene (Sizun et al. 2010) suggest a different energy partition: $f_{\rm kin} \approx 0.1$, $f_{\rm gr} \approx 0.2$, and $f_{\rm int} \approx 0.6$ (distributed over vibrational levels with $v \approx 4$–6), the rest of the energy being spent to overcome the chemical bound potential well. For low densities, the energy converted into heating is then $\langle E_{\rm form}\rangle \approx 0.5$ eV. If, on the other hand, the ambient density is sufficiently high to collisionally de-excite the newly formed H_2 molecules, $n_{\rm H} \gtrsim 10^6$ cm^{-3}, the energy available for heating the gas per H_2 formation is $\langle E_{\rm form}\rangle = (f_{\rm kin} + f_{\rm int}) E_{\rm HH} \approx 3.1$ eV. For a dense PDR, Le Bourlot et al. (2012) show that H_2 formation heating dominates over photoelectric heating at the edge of the cloud, especially for high gas temperatures (of the order of a few 100 K). Similarly, we see this process often dominating the heating in the warm surfaces of planet-forming disks (temperatures again of the order of $\sim 100 - 300$ K).

1.2 COOLING PROCESSES

1.2.1 Adiabatic expansion

As mentioned in Sect. 1.1.5, shocks occur frequently in the hot and warm ionized medium. The gas behind such a shock will expand adiabatically ($pV^\gamma = $ const), leading to cooling

$$\Lambda_{\rm ad} = \frac{p}{V}\frac{{\rm d}V}{{\rm d}t} \quad . \tag{1.31}$$

However, adiabatic expansion cooling will likely not dominate the heating/cooling balance, see for example the detailed study on heating/cooling in protoplanetary disk winds of Sellek et al. (2022) and also Chap. **??** on hydrodynamics.

1.2.2 Free-free emission

In media with a large ionization fraction, free electrons can scatter off the ions. In this process, the electrons lose energy (change of momentum in the electric field of the ion) and this energy is radiated away in a process called free-free emission, leading to a continuous spectrum. If the electron has a velocity distribution $f_e(v)$, the emissivity for this radiation can be calculated as

$$\epsilon_{\rm ff}(\nu) = \frac{n_e}{4\pi}\int P(\nu, v) f_e(v)\,{\rm d}v \tag{1.32}$$

where $P(\nu, v)$ is the power emitted at frequency ν in a scattering event with an electron density n_e and a velocity v. Using the Maxwell-Boltzmann velocity

distribution, this yields

$$\epsilon_{\rm ff}(\nu) = \frac{8}{3}\left(\frac{2\pi}{3}\right)^{1/2} \frac{e^6}{m_e^2 c^3}\left(\frac{m_e}{kT_e}\right)^{1/2} Z_i^2 n_i n_e g_{\rm ff}(\nu, T_e)\exp(-h\nu/k_{\rm B}T_e) \ . \quad (1.33)$$

Here, the elementary charge e is in cgs units, and $g_{\rm ff}$ is the Gaunt factor for free-free emission which captures quantum effects, and T_e is the electron temperature. For electron-proton scattering at high frequencies, $\nu \gg 10^{14}$ Hz, this factor approaches unity. The cooling rate of the gas (in erg cm^{-3} s^{-1}) is obtained by integrating over the emissivity and the solid angle

$$\Lambda_{\rm ff} = 4\pi \int_0^\infty \epsilon_{\rm ff}(\nu)\,{\rm d}\nu. \ . \quad (1.34)$$

1.2.3 Radiative recombination cooling

Radiative recombination is the inverse process of photoionisation. In this process, the kinetic energy of the electron will be radiated away, thus cooling the gas. For a gas where hydrogen is predominantly ionized, this cooling rate (in erg cm^{-3} s^{-1}) can be written as

$$\Lambda_{\rm rr} = n_e n_p \alpha \langle E_{\rm rr}\,,\rangle \quad (1.35)$$

with $\langle E_{\rm rr}\rangle$ the average energy emitted per recombining electron. Assuming that the recombination cross section can be approximated by a power law $\propto E^p$ (similar to what we saw for photoionization), we obtain for $\langle E_{\rm rr}\rangle$ in the optically thin (case A) and thick (case B) limit

$$\langle E_{\rm rr}\rangle_{\rm A} = \left[0.787 - 0.0230\,\ln(T_4/Z^2)\right] k_{\rm B}T \quad (1.36)$$

$$\langle E_{\rm rr}\rangle_{\rm B} = \left[0.684 - 0.0416\,\ln(T_4/Z^2)\right] k_{\rm B}T \ . \quad (1.37)$$

1.2.4 Radiative line cooling

An energy level of an atom or ion can be populated by collisions, a process that extracts kinetic energy from the gas. If such a collisional excitation is followed by a collisional de-excitation, there is no net energy loss. If however, the timescale for spontaneous emission of a photon is shorter than that for collisional de-excitation, then the energy can be radiated away and will be lost from the gas if it is optically thin to radiation of that frequency. The level populations have to be calculated from statistical equilibrium using the collisional excitation rate of the relevant collision partners. Depending on the species considered and the degree of ionisation, electrons or hydrogen atoms dominate the collisional excitation rates.

At high temperatures of $T \approx 10^4$ K, those collisions provide enough kinetic energy ($k_{\rm B}T$) to excite the $n = 2$ level of hydrogen if it is not fully ionized.

In that case, Ly-α will become an important cooling line. In general, at high gas temperatures, most of the cooling originates from electronic transitions of metal ions (O III, O II, S III) which occur in the UV, optical and near-IR wavelength range. For lower temperatures, the kinetic energy of collisions can no longer excite electronic levels and the cooling will be restricted to fine structure line in the ground electronic states of abundant ions, e.g. [S III] 18.7 μm, [Ne II] 12.8 μm, emitting at mid- and far-IR wavelengths.

1.2.4.1 General form of the radiative heating and cooling functions

Consider a species s with density n_s interacting by collisions with species k, each with density n_k, and exposed to a radiation field with specific intensity J_ν. Assume, for simplicity, that the species s has only two energy levels (it can be electronic, vibrational or rotational): level i with energy E_i and level j with energy $E_j > E_i$. Collisional excitation of s from a level i to level j at the rate C_{ij} followed by radiative decay of level j at the rate R_{ji} results in the loss from the gas of an amount of kinetic energy $E_j - E_i$ (*radiative cooling*). The rate of radiative de-excitation, including stimulated emission by the radiation field, is

$$R_{ji} = A_{ji} + B_{ji} J_\nu, \tag{1.38}$$

where A_{ji} and B_{ji} are the Einstein coefficients, and J_ν is the spectral energy density of the radiation field at the frequency ν corresponding to the transition i–j. The rate of collisional excitation, summed over all the collision partners k (also including the species s itself) is $C_{ij} = n \sum_k x_k \gamma_{k,ij}$, where $\gamma_{k,ij}$ is the *collisional coefficient* (with units of cm^3 s^{-1} in cgs), $n = \sum_k n_k$ is the total density, and $x_k = n_k/n$ is the fractional abundance of species k. However, level j can also be collisionally de-excited to level i at a rate C_{ji}. In this case, no energy is lost by the gas. Defining the probability of radiative de-excitation of level j to level i as

$$\mathcal{P}^{\rm r}_{ji} = \frac{R_{ji}}{R_{ji} + C_{ji}}, \tag{1.39}$$

the energy lost by the gas per unit time and unit volume via this transition is

$$\Lambda_{s,ij} = n_{s,i} C_{ij} \mathcal{P}^{\rm r}_{ji} (E_j - E_i) \equiv n n_s \mathcal{L}_{s,ij}, \tag{1.40}$$

where $n_{s,i}$ is the density of species s in the level i, and $\mathcal{L}_{s,ij}$ is the *cooling function* relative to the transition i–j. In cgs units, the units of $\mathcal{L}_{s,ij}$ are erg cm^3 s^{-1}. Similarly, it is possible to define a *heating function* $\mathcal{G}_{s,ij}$ (also with units of erg cm^3 s^{-1}) by considering the radiative excitation of a transition i–j followed by its collisional de-excitation. In this case, the energy gained by the gas per unit of time and volume is

$$\Gamma_{s,ij} = n_{s,i} R_{ij} \mathcal{P}^{\rm c}_{ji} (E_j - E_i) \equiv n n_s \mathcal{G}_{s,ij}, \tag{1.41}$$

where $R_{ij} = B_{ij} u_{ij}$ and

$$\mathcal{P}^{\rm c}_{ji} = \frac{C_{ji}}{R_{ji} + C_{ji}} \tag{1.42}$$

is the probability of collisional de-excitation of level j to level i, with $C_{ji} = n \sum_k x_k \gamma_{k,ji}$. The general form of the *net cooling function* is then

$$\mathcal{L}_{s,ij} - \mathcal{G}_{s,ij} = x_{s,i} \frac{G_{ij} R_{ji} - R_{ij} G_{ji}}{R_{ji} + n G_{ji}} (E_j - E_i), \tag{1.43}$$

where $x_{s,i} = n_{s,i}/n_s$, and, for brevity, $G_{ij} = \sum_k x_k \gamma_{k,ij}$ and similarly for G_{ji}. The evaluation of the net cooling function thus requires the knowledge of the gas composition x_k, of the level population of each species $x_{s,i}$ of the collisional excitation and de-excitation coefficients $\gamma_{k,ij}$ and $\gamma_{k,ji}$, of the Einstein coefficients A_{ji}, and of the radiation field J_ν. If the latter is a black body with temperature $T_{\rm rad}$, the total net cooling function is a function of n, T, and $T_{\rm rad}$. Notice that $\mathcal{L}_{s,ij} - \mathcal{G}_{s,ij}$ can be positive (*net cooling*) or negative (*net heating*). The latter case occurs for example in the post-recombination Universe, where a tiny amount of molecules (mostly H_2 and HD) transfer energy from the "photon fluid" (the CMB) with temperature $T_{\rm rad}$ to the cooler gas with temperature T.
In the absence of a radiation field, or whenever radiative excitation and stimulated emission can be neglected, the net cooling function can be simplified by setting $R_{ij} = 0$ and $R_{ji} = A_{ji}$. In this case,

$$\mathcal{L}_{s,ij} - \mathcal{G}_{s,ij} = x_{s,i} \frac{G_{ij} A_{ji}}{A_{ji} + n G_{ji}} (E_j - E_i) = \frac{1}{1 + n/n_{ji}^{\rm cr}} x_{s,i} G_{ij} (E_j - E_i), \tag{1.44}$$

where we have defined the *critical density* of the transition $n_{ji}^{\rm cr} \equiv A_{ji}/G_{ji}$.
It is instructive to consider two limiting cases: (*i*) the low density limit $n \ll n_{ji}^{\rm cr}$, and (*ii*) the high density limit $n \gg n_{ji}^{\rm cr}$. In the low-density limit, the net cooling function becomes

$$(\mathcal{L}_{s,ij} - \mathcal{G}_{s,ij})_{\rm low} = x_{s,i} G_{ji} (E_j - E_i), \tag{1.45}$$

and is only a function of the gas temperature T, since the level populations $x_{s,i}$ and the collisional rate coefficients G_{ji} only depend on T (for a given composition). In the high-density limit, the net cooling function becomes inversely proportional to density,

$$(\mathcal{L}_{s,ij} - \mathcal{G}_{s,ij})_{\rm high} = \frac{1}{n} x_{s,i} A_{ji} (E_j - E_i). \tag{1.46}$$

Thus, for example, the energy radiated per unit time $n(\mathcal{L}_{s,ij} - \mathcal{G}_{s,ij})$ by a contracting molecular cloud initially increases proportionally to the density n, as long as $n \ll n_{ji}^{\rm cr}$, allowing the cloud temperature to remain approximately constant, but eventually it saturates to a value independent on density as $n \to n_{ji}^{\rm cr}$, and cooling becomes inefficient.

1.2.4.2 Net cooling in the LTE limit

The net cooling function Eq. (1.44) can also be expressed in terms of the fractional population of the upper level j. For a two-level species, in the absence of

an external radiation field, the equation of statistical equilibrium simplifies to

$$x_{s,j}(A_{ji} + nG_{ji}) = x_{s,i} nG_{ij}, \tag{1.47}$$

and Eq. (1.44) becomes

$$n(\mathcal{L}_{s,ij} - \mathcal{G}_{s,ij}) = x_{s,j} A_{ji}(E_j - E_i), \tag{1.48}$$

an expression frequently adopted to evaluate the total net cooling function Eq. (1.56). In the LTE limit, when the density is larger than the critical density for all transitions, the level populations are given by a Boltzmann distribution at the local kinetic temperature T, and

$$x_{s,j}(T) = \frac{g_j \exp(-E_j/k_{\rm B}T)}{Z_s(T)}, \tag{1.49}$$

where g_j is the level degeneracy and $Z_s(T) = \sum_j g_j \exp(-E_j/k_{\rm B}T)$ is the partition function. Thus, $n(\mathcal{L}_{s,ij} - \mathcal{G}_{s,ij})_{\rm LTE}$ only depends on T.

1.2.4.3 Escape probability

The expression above for the net cooling rate, Eq. (1.43), assumes that that the optical depth in each transition of interest is negligible, so that photons emitted in spontaneous transitions escape from the medium, rather than being reabsorbed. When the optical depth is not negligible, the opacity of the line must be taken into account. In an optically thick transition, the emitted photon bounces around until it eventually escapes. This radiative trapping increases the population of the upper state j and thus increases the rate of collisional de-excitation, which in turn decreases the cooling rate. In a medium where the velocity gradient $|{\rm d}v/{\rm d}z|$ is large, the *Sobolev approximation*[8] (Sobolev 1960), or *large velocity gradient* (LVG) approximation, gives the *escape probability* of a photon in any direction $\hat{\mathbf{k}}$,

$$\beta_{ij}(\hat{\mathbf{k}}) = \frac{1 - \exp[-\tau_{ij}(\hat{\mathbf{k}})]}{\tau_{ij}(\hat{\mathbf{k}})}, \tag{1.50}$$

where the line-integrated Sobolev optical depth[9] is defined as

$$\tau_{ij}(\hat{\mathbf{k}}) = \frac{hcn}{4\pi|{\rm d}v/{\rm d}z|_{\hat{\mathbf{k}}}}(x_i B_{ij} - x_j B_{ji}), \tag{1.51}$$

where the subscript s indicating the species has been omitted for simplicity. The net cooling Eq. (1.43) is then reduced by an amount $\beta_{ij} = \langle\beta_{ij}(\hat{\mathbf{k}})\rangle$, equal to

8. The essence of this *local approximation* is that for large velocity gradients, "the intensity at frequency ν only changes at discrete resonance points where the material has just the right Doppler shift to allow it to absorb and emit at frequency ν. Therefore the problem of determining the intensities reduces to the simpler one of determining the variation of intensity in the neighborhood of a single resonance point" (Rybicki & Hummer 1978).
9. If the absorbers have a gaussian velocity distribution (gaussian line profile), the line-center optical depth is a factor of $\pi^{1/2}$ smaller than the line-integrated optical depth.

escape probability angle-averaged (or density-averaged) over all the directions[10]. The same reduction of course must be applied to the radiative decay coefficients R_{ji} in the equations of statistical equilibrium for the level populations, and to the critical density for an excited state. Exact formulae for β_{ij} in a plane-parallel geometry with an arbitrary velocity gradient are given by Hummer & Rybicki (1982). Several approximated expressions for β_{ij} for a plane-parallel cloud geometry can be found in the literature. Care must be taken to distinguish the *one-sided* escape probability (which approaches $1/2$ in the limit of small optical depth), valid when photons can escape only through one face of the cloud, from the *cloud-center* escape probability (which approaches unity in the limit of small optical depth). An approximated expression for the former is given by de Jong et al. (1980) (also adopted by Tielens & Hollenbach 1985),

$$\beta_{ij} = \begin{cases} \frac{1-\exp(-2.34\tau_{ij})}{4.68\tau_{ij}} & \text{for } \tau_{ij} < 7 \\ \frac{1}{4\tau_{ij}[\ln(\tau_{ij}/\sqrt{\pi})]^{1/2}} & \text{for } \tau_{ij} \geq 7. \end{cases} \tag{1.52}$$

whereas the latter is given by Hollenbach & McKee (1979)[11]

$$\beta_{s,ij} = \frac{1}{1+\tau_{ij}/\sqrt{\pi}[2\pi\ln(2.13+\tau_{ij}^2/\pi)]^{1/2}}. \tag{1.53}$$

Other approximated expressions are given by Scoville & Solomon (1974) and Neufeld & Kaufman (1993). Draine (2011) gives an approximation for β_{ij} in a spherical homogeneous cloud.

Absorption by dust, when it is not negligible, is assumed to be equivalent to escape since the absorbed line photon is converted to an infrared continuum photon, which can freely escape from the medium. Hollenbach & McKee (1979) give a simple approximate expression for the direction-averaged escape probability corrected for dust absorption,

$$\beta_{ij}^{\rm tot} \approx \delta_{ij} + \frac{(1-\delta_{ij})\exp(-\tau_{\rm d})}{1+(1-\delta_{ij})\tau_{\rm d}^2}\beta_{ij}, \tag{1.54}$$

where $\tau_{\rm d}$ is the optical depth due to the dust at the frequency of the transition, and

$$\delta_{ij} \approx \frac{2(\tau_{\rm d}/\pi^{1/2}\tau_{ij})}{1+2(\tau_{\rm d}/\pi^{1/2}\tau_{ij})}\left[\ln\left(2.72+\frac{\tau_{ij}}{\tau_{\rm d}}\right)\right]^{1/2}, \tag{1.55}$$

is the probability per scattering that the photon will be absorbed by dust.

The evaluation of the total cooling function proceeds with the solution of the equations of statistical equilibrium of the level populations for each species s

10.In a disk geometry, the optical depth used to compute the escape probability is the optical depth in the vertical direction, where the photons most readily escape.

11.Note that the original expression is written in terms of the line-center optical depth.

followed by a sum over all the levels of the rate of escaping radiation given by Eq. (1.43) in the general case or Eq. (1.44) in the absence of a radiation field, multiplied by the escape probabilities given by Eq. (1.54), and summed over all species s present in the gas (generally given a specific chemical model):

$$\mathcal{L} - \mathcal{G} = \sum_s \sum_{j,i<j} (\mathcal{L}_{s,ij} - \mathcal{G}_{s,ij}) \beta_{s,ij}. \tag{1.56}$$

In the LTE limit, the level populations are given by the Boltzmann distribution (1.49), and the total cooling function takes the form

$$(\mathcal{L} - \mathcal{G})_{\rm LTE} = \frac{1}{n} \sum_s \sum_{j,i<j} \frac{g_j \exp(-E_j/k_{\rm B}T)}{Z_s(T)} A_{ji} (E_j - E_i) \beta_{s,ij}. \tag{1.57}$$

1.2.5 Cooling rates: special cases

Analytical and numerical expressions useful to evaluate the radiative cooling rate of a gas in different physical conditions have been computed or tabulated in several papers. Some of them are described in the following sections alongside relevant papers containing useful analytical formulae or numerical tables.

1.2.5.1 Cooling of molecular gas

Comprehensive studies of radiative cooling in dense molecular gas have been carried out by Goldsmith & Langer (1978) and Neufeld et al. (1995).

• Neufeld et al. (1995) include a detailed treatment of the chemistry and excitation of H_2, CO, H_2O, HCl, O_2, C, O, and their isotopic variants. The results cover the range 10^3 cm$^{-3} \lesssim n(H_2) \lesssim 10^{10}$ cm^{-3} and 10 K $\lesssim T \lesssim$ 2500 K, but no fitting functions are given. Fig. 1.2 shows the cooling rate of Neufeld et al. (1995) as a function of density and temperature.

• Goldsmith (2001) gives an approximate analytical fitting formula of the total cooling function of Goldsmith & Langer (1978) that includes the contribution of CO and its isotopologues, C, CS, and H_2O. The cooling rate (in erg cm^{-3} s^{-1}) is parametrized as

$$\Lambda = \alpha \left(\frac{T}{10\ {\rm K}} \right)^{\beta}, \tag{1.58}$$

where α and β are functions of the density $n(H_2)$, depletion factor δ, and velocity gradient dv/dr. The values of α and β are tabulated in Table 4 of Goldsmith (2001) for $dv/dr = 1$ km s^{-1} pc^{-1} and various values of δ. They can be fitted by polynomials in $\log n(H_2)$,

$$\log \alpha = \sum_{k=0}^{N} a_k [\log n(H_2)]^k, \qquad \beta = \sum_{k=0}^{N} b_k [\log n(H_2)]^k, \tag{1.59}$$

with the coefficients a_k and b_k listed in Tab. 1.2. Eqs. (1.58)–(1.59) are valid for 5 K $\lesssim T \lesssim$ 30 K and 5×10^2 cm$^{-3} \lesssim n(H_2) \lesssim 5 \times 10^6$ cm^{-3}.

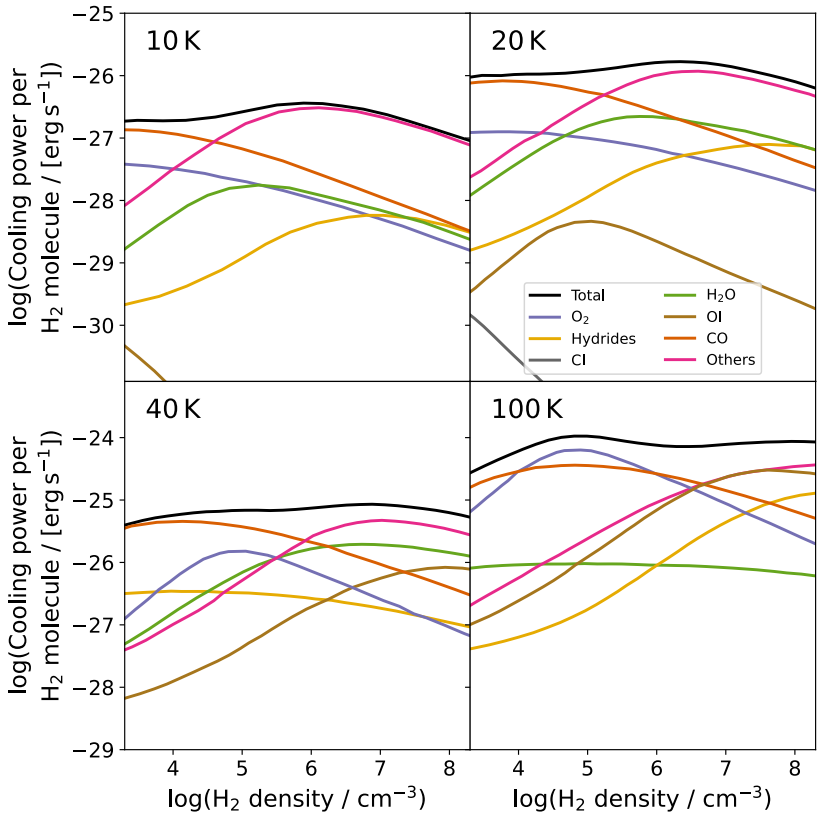

FIGURE 1.2 Cooling power (in erg s^{-1}) as a function of temperature and density in a molecular cloud (from Neufeld et al. 1995).

• Whitworth & Jaffa (2018) give the following analytical fit for the cooling rate (in erg cm^{-3} s^{-1}) of CO and its isotopologues,

$$\Lambda_{\rm CO} = (\Lambda_{\rm CO,low}^{-1/\beta} + \Lambda_{\rm CO,high}^{-1/\beta})^{-\beta}, \tag{1.60}$$

where

$$\Lambda_{\rm CO,low} = A X_{\rm CO} \rho^2 c_{\rm s}^3 \tag{1.61}$$

is the cooling rate in the low-density optically thin limit,

$$\Lambda_{\rm CO,high} = B|\nabla \cdot \mathbf{u}| c_{\rm s}^8 \tag{1.62}$$

is the cooling rate in the high-density optically thick limit (in the LVG approximation, see Sect. 1.2.4.3), and

$$\beta = 0.813 \left(\frac{\rho}{\rm g\ cm^{-3}}\right)^{0.0533} \left(\frac{c_{\rm s}}{\rm cm^2\ s^{-1}}\right)^{0.328}. \tag{1.63}$$

TABLE 1.2 Numerical values of coefficients a_k and b_k in Eq. (1.59).

	$\delta = 0$		$\delta = 1$		$\delta = 3$		$\delta = 10$	
k	a_k	b_k	a_k	b_k	a_k	b_k	a_k	b_k
0	−28.94	−2.581	−27.56	1.865	−27.80	0.090	−28.81	−0.645
1	2.444	2.856	1.500	0.830	1.500	0.830	1.815	1.805
2	−0.306	−0.511	−0.100	0.050	−0.100	−0.050	−0.125	−0.075
3	0.0137	0.0333						
	$\delta = 30$		$\delta = 100$					
k	a_k	b_k	a_k	b_k				
0	−29.77	−0.875	−30.65	−0.025				
1	2.110	1.125	2.385	0.675				
2	−0.150	−0.075	−0.175	−0.025				

Here, $X_{\rm CO}$ is the CO abundance, ρ is the gas density, $c_{\rm s}$ is the sound speed, $\nabla \cdot \mathbf{u}$ is the velocity divergence, A and B are two-dimensional constants, $A = 4.63 \times 10^8$ cm^2 g^{-1}, and $B = 4.58 \times 10^{-45}$ cm^{-9} g s^6. Eq. (1.60)–(1.63) are valid for 10 K $\lesssim T \lesssim$ 100 K and 3×10^2 cm^{-3} $\lesssim n({\rm H_2}) \lesssim 3 \times 10^5$ cm^{-3}.

1.2.5.2 *Cooling of hot plasma, non-equilibrium cooling*

As discussed in Sect. 1.1.5.3, hot ($\gtrsim 10^6$ K) gas is produced within galaxies by fast stellar winds and supernovae, and is maintained at even higher temperatures ($\sim 10^7$–10^8 K) in the intergalactic medium within galaxy clusters, probably by feedback from active galactic nuclei at cluster centers. Therefore, the radiative cooling of a hot, optically thin, low-density plasma has received considerable attention, and is a fundamental ingredient of models of interstellar shocks and galaxy formation.

Traditionally, a distinction is made between a *low-T* ($T \lesssim 10^4$ K) and a *high-T* ($T \gtrsim 10^4$ K) cooling rate, due to complexities arising in the low-T regime from the transition to neutral gas and the formation of molecules. Very often, calculations of the high-T cooling rate of a hot plasma have assumed *collisional ionization equilibrium* (CIE), a condition that applies when the cooling time scale is longer than the recombination time scale. However, gas below $\sim 10^6$ K is generally not in ionization equilibrium because it is cooling faster than it is recombining, as first pointed out by Kafatos (1973) and Shapiro & Moore (1976). The effect of this *non-equilibrium cooling* is to leave behind a greater residual of free electrons and ions, as compared to the equilibrium case. This deviation from equilibrium ionization leads to a cooling rate different from the CIE case. Self-consistent calculations of non-equilibrium (time-dependent) cooling rates for a dust-free gas in wide temperature (10 K $\le T \le 10^8$ K) and metallicity ($10^{-4} Z_\odot \le Z \le 2\, Z_\odot$) ranges are given by Vasiliev (2013).

A shock-heated gas is relatively inefficient at radiatively cooling below $\sim 10^4$ K, due to the scarcity of free electrons and the exponential cutoff in the temperature

dependence of the Ly-α excitation (the so-called Ly-α *barrier*). In this low-T regime, cooling is ensured by metals and molecules. However, is usually assumed that behind a strong shock ($v_s \sim 10^2$–10^3 km s^{-1}), all pre-existing molecules are dissociated and dust grains are destroyed (Draine & Salpeter 1979). The cooling rate in these conditions then depends on the release in the gas of metals previously locked onto dust grains, and the efficiency of gas-phase reactions to reform molecules. If a significant fraction of dust grains survives behind the shock, it can efficiently catalyze the formation of H_2 by grain-surface reactions. In either case, the kinetic rate equations with multi–species chemistry must be solved in non-equilibrium and self–consistently with the dynamical evolution of the medium.

• Wang et al. (2014) provide tables, a C++, and a PYTHON routine[12] that evaluates the CIE cooling rate over a large range of metallicity ($Z < 30\,Z_\odot$) and density ($n_H < 10^{12}$ cm^{-3}).

1.2.5.3 Cooling of a gas of primordial composition

For a review of the thermodynamics and chemistry of a gas of primordial composition see Galli & Palla (2013) and Bovino & Galli (2019). Extensive and accurate analytical parametrizations of cooling functions and cooling rates, and their ranges of validity, can be found in the papers listed below.

• Glover (2015) presents a comparison of H_2-H cooling functions adopted in numerical models of primordial gas: Martin et al. (1996), Galli & Palla (1998) and Glover & Abel (2008) in the low-density limit, Hollenbach & McKee (1979) and Glover (2015) in LTE. Polynomial fits are provided for each case. In the LTE limit, valid for $T \lesssim 100$ K or $n(H) \gtrsim 10^6$ cm^{-3}, the cooling rate (in erg s^{-1}) is independent on the density.

• Flower et al. (2021) evaluates the cooling function of H_2 for collisions with He, H^+, and H_2 and provide useful numerical routines in the range 10^2 K $\lesssim T \lesssim 2 \times 10^4$ K and 1 cm^{-3} $\lesssim n(H) \lesssim 10^6$ cm^{-3}. A polynomial approximation is given for the cooling rate in the LTE limit.

• Scholz & Walters (1991) and Cen (1992) give analytical expressions for the cooling function arising from H-e collisions (commonly referred to simply as *Ly-α cooling*).

• Lipovka et al. (2005) give a double-polynomial fit for the HD-H cooling function valid in the range 10^2 K $\lesssim T \lesssim 2 \times 10^4$ K and 1 cm^{-3} $\lesssim n(H) \lesssim 10^8$ cm^{-3}.

• Coppola et al. (2011) give polynomial fits of the cooling rates of HD, HD^+, HeH^+, LiH, and LiH^+ in the LTE limit in the temperature range 10 K $\lesssim T \lesssim 10^4$ K.

• Glover & Savin (2009) give analytical fits of the cooling function of H_3^+ in the low-density and LTE limit. The cooling rate in the latter case has been calculated and fitted also by Miller et al. (2010).

12. https://github.com/wangye0206/Cloudy_Helper

1.3 SOLVING THE HEATING/COOLING BALANCE

The main purpose of modelling individual heating/cooling processes is to self-consistently determine the gas temperature. Following Woitke (2015) we consider the first law of thermodynamics

$$\boxed{\frac{\mathrm{d}(\rho e)}{\mathrm{d}t} = -p\frac{\mathrm{d}V}{\mathrm{d}t} + \sum_i \rho\Gamma_i - \sum_k \rho\Lambda_k\,,} \tag{1.64}$$

with e being the internal energy in units of $\mathrm{erg\,cm^{-3}}$, p the gas pressure in $\mathrm{erg\,cm^{-3}}$, $V = 1/\rho$ the specific volume and ρ the mass density $\mathrm{g\,cm^{-3}}$. Γ_i and Λ_k are the various heating and cooling rates per unit volume discussed in this chapter.

The $-pdV$ work is often not significant and can be neglected (see Sect. 1.2.1), it also requires proper coupling of heating/cooling to dynamical processes and therefore can become computationally expensive (see also Chap. **??**). Here we assume that heating/cooling will be rapid; in that case one can simplify eq. (1.64) by assuming thermal energy equilibrium:

$$\boxed{\sum_i \Gamma_i(T, n_{\mathrm{sp}}) - \sum_k \Lambda_k(T, n_{\mathrm{sp}}) = 0.} \tag{1.65}$$

As the various heating and cooling processes depend on temperature and the chemical species densities, Eq. (1.65) has to be solved iteratively with the chemistry by varying T. However, as this is often computationally too expensive, especially in dynamical simulations, (semi)analytical approximations or tabulated numbers (Sect. 1.2.5 are used and Chap. **??** for more details).

BIBLIOGRAPHY

Aikawa, Y. & Nomura, H. 2006, ApJ, 642, 1152

Aresu, G., Kamp, I., Meijerink, R., et al. 2011, A&A, 526, A163

Bakes, E. L. O. & Tielens, A. G. G. M. 1994, ApJ, 427, 822

Bethell, T. J. & Bergin, E. A. 2011, ApJ, 740, 7

Bovino, S. & Galli, D. 2019, in Formation of the First Black Holes, ed. M. Latif & D. Schleicher, 45–66

Cen, R. 1992, ApJS, 78, 341

Cleeves, L. I., Bergin, E. A., Qi, C., Adams, F. C., & Öberg, K. I. 2015, ApJ, 799, 204

Coppola, C. M., Lodi, L., & Tennyson, J. 2011, MNRAS, 415, 487

D'Alessio, P., Cantö, J., Calvet, N., & Lizano, S. 1998, ApJ, 500, 411

Dalgarno, A., Yan, M., & Liu, W. 1999, ApJS, 125, 237

de Jong, T., Boland, W., & Dalgarno, A. 1980, A&A, 91, 68

Dolag, K., Borgani, S., Schindler, S., Diaferio, A., & Bykov, A. M. 2008, Space Sci. Rev., 134, 229

Draine, B. T. 1978, ApJS, 36, 595

Draine, B. T. 2003, ApJ, 598, 1026

Draine, B. T. 2011, Physics of the Interstellar and Intergalactic Medium (Princeton: Princeton University Press)
Draine, B. T. & Li, A. 2001, ApJ, 551, 807
Draine, B. T. & Li, A. 2007, ApJ, 657, 810
Draine, B. T. & Salpeter, E. E. 1979, ApJ, 231, 438
Du, F. & Bergin, E. A. 2014, ApJ, 792, 2
Ercolano, B., Drake, J. J., Raymond, J. C., & Clarke, C. C. 2008, ApJ, 688, 398
Field, G. B., Goldsmith, D. W., & Habing, H. J. 1969, ApJ, 155, L149
Flower, D. R. & Pineau des Forêts, G. 2003, MNRAS, 343, 390
Flower, D. R., Pineau des Forêts, G., Hily-Blant, P., et al. 2021, MNRAS, 507, 3564
Furlanetto, S. R. & Stoever, S. J. 2010, MNRAS, 404, 1869
Galli, D. & Palla, F. 1998, A&A, 335, 403
Galli, D. & Palla, F. 2013, ARA&A, 51, 163
Glassgold, A. E., Galli, D., & Padovani, M. 2012, ApJ, 756, 157
Glassgold, A. E. & Langer, W. D. 1973, ApJ, 186, 859
Glassgold, A. E. & Langer, W. D. 1974, ApJ, 193, 73
Glassgold, A. E. & Najita, J. R. 2015, ApJ, 810, 125
Glover, S. C. O. 2015, MNRAS, 453, 2901
Glover, S. C. O. & Abel, T. 2008, MNRAS, 388, 1627
Glover, S. C. O. & Savin, D. W. 2009, MNRAS, 393, 911
Goldsmith, P. F. 2001, ApJ, 557, 736
Goldsmith, P. F. & Langer, W. D. 1978, ApJ, 222, 881
Gorti, U. & Hollenbach, D. 2004, ApJ, 613, 424
Harten, A. & Hyman, J. M. 1983, Journal of Computational Physics, 50, 235
Heays, A. N., Bosman, A. D., & van Dishoeck, E. F. 2017, A&A, 602, A105
Hollenbach, D. & McKee, C. F. 1979, ApJS, 41, 555
Hummer, D. G. & Rybicki, G. B. 1982, ApJ, 254, 767
Igea, J. & Glassgold, A. E. 1999, ApJ, 518, 848
Jonkheid, B., Faas, F. G. A., van Zadelhoff, G. J., & van Dishoeck, E. F. 2004, A&A, 428, 511
Kafatos, M. 1973, ApJ, 182, 433
Kamp, I. & Dullemond, C. P. 2004, ApJ, 615, 991
Kamp, I. & van Zadelhoff, G. J. 2001, A&A, 373, 641
Le Bourlot, J., Le Petit, F., Pinto, C., Roueff, E., & Roy, F. 2012, A&A, 541, A76
Le Teuff, Y. H., Millar, T. J., & Markwick, A. J. 2000, A&AS, 146, 157
Lipovka, A., Núñez-López, R., & Avila-Reese, V. 2005, MNRAS, 361, 850
Liszt, H. S. 2007, A&A, 461, 205
Liu, X. & Shemansky, D. E. 2012, Journal of Physics B Atomic Molecular Physics, 45, 095203
Martin, P. G., Schwarz, D. H., & Mandy, M. E. 1996, ApJ, 461, 265
Miller, S., Stallard, T., Melin, H., & Tennyson, J. 2010, Faraday Discussions, 147, 283
Monaghan, J. J. & Gingold, R. A. 1983, Journal of Computational Physics, 52, 374
Neufeld, D. A. & Kaufman, M. J. 1993, ApJ, 418, 263
Neufeld, D. A., Lepp, S., & Melnick, G. J. 1995, ApJS, 100, 132
Osterbrock, D. E. & Ferland, G. J. 2006, Astrophysics of gaseous nebulae and active galactic nuclei
Pringle, J. E. 1981, ARA&A, 19, 137
Rab, C., Güdel, M., Woitke, P., et al. 2018, A&A, 609, A91
Rozwadowska, K., Vissani, F., & Cappellaro, E. 2021, New A, 83, 101498
Rybicki, G. B. & Hummer, D. G. 1978, ApJ, 219, 654
Scalo, J. M. 1977, ApJ, 213, 705

Schatzman, E. 1949, Annales d'Astrophysique, 12, 203
Scholz, T. T. & Walters, H. R. J. 1991, ApJ, 380, 302
Schoonjans, T., Brunetti, A., Golosio, B., et al. 2011, Spectrochimica Acta, 66, 776
Scoville, N. Z. & Solomon, P. M. 1974, ApJ, 187, L67
Sellek, A. D., Clarke, C. J., & Ercolano, B. 2022, MNRAS, 514, 535
Shakura, N. I. & Sunyaev, R. A. 1973, A&A, 24, 337
Shapiro, P. R. & Moore, R. T. 1976, ApJ, 207, 460
Shull, J. M. & van Steenberg, M. E. 1985, ApJ, 298, 268
Sizun, M., Bachellerie, D., Aguillon, F., & Sidis, V. 2010, Chemical Physics Letters, 498, 32
Sobolev, V. V. 1960, Moving envelopes of stars
Spitzer, Lyman, J. & Tomasko, M. G. 1968, ApJ, 152, 971
Thornton, K., Gaudlitz, M., Janka, H. T., & Steinmetz, M. 1998, ApJ, 500, 95
Tielens, A. G. G. M. & Hollenbach, D. 1985, ApJ, 291, 722
Vasiliev, E. O. 2013, MNRAS, 431, 638
Verner, D. A., Ferland, G. J., Korista, K. T., & Yakovlev, D. G. 1996, ApJ, 465, 487
Verner, D. A. & Yakovlev, D. G. 1995, A&AS, 109, 125
Wang, Y., Ferland, G. J., Lykins, M. L., et al. 2014, MNRAS, 440, 3100
Watson, W. D. 1972, ApJ, 176, 103
Weingartner, J. C. & Draine, B. T. 2001a, ApJ, 548, 296
Weingartner, J. C. & Draine, B. T. 2001b, ApJS, 134, 263
Weingartner, J. C., Draine, B. T., & Barr, D. K. 2006, ApJ, 645, 1188
Weymann, R. 1960, ApJ, 132, 452
Whitworth, A. P. & Jaffa, S. E. 2018, A&A, 611, A20
Woitke, P. 2015, in European Physical Journal Web of Conferences, Vol. 102, European Physical Journal Web of Conferences, 00011
Woitke, P., Kamp, I., & Thi, W. F. 2009, A&A, 501, 383
Woitke, P., Riaz, B., Duchêne, G., et al. 2011, A&A, 534, A44
Wolfire, M. G., Tielens, A. G. G. M., Hollenbach, D., & Kaufman, M. J. 2008, ApJ, 680, 384
Woodward, P. & Colella, P. 1984, Journal of Computational Physics, 54, 115
Xu, Y. & McCray, R. 1991, ApJ, 375, 190
Yan, M., Sadeghpour, H. R., & Dalgarno, A. 2001, ApJ, 559, 1194